PRE- PRINT VERSION _ UNICA HTTPS://DOI.ORG/10.1016/J.BMC.2023.117376

Versatile anti-infective properties of pyrido- and dihydropyrido[2,3-*d*]pyrimidine-based compounds

Ibrahim S. Al Nasr,[a,b] Angela Corona,[c] Waleed S. Koko,[b] Tariq A. Khan,[d] Ridha Ben Said,[e,f] Ismail Daoud,[g,h] Seyfeddine Rahali,[f] Enzo Tramontano,[c] Rainer Schobert,[i] Noureddine Amdouni,[e] Bernhard Biersack[i,*]

[a]*Department of Biology, College of Science and Arts, Qassim University, Unaizah 51911, Saudi Arabia*

[b]*Department of Science Laboratories, College of Science and Arts, Qassim University, King Abdelaziz Road, Ar Rass 51921, Saudi Arabia*

[c]*Laboratorio di Virologia Molecolare, Dipartimento di Scienze della Vita e Dell'Ambiente, Universitá degli Studi di Cagliari, Cittadella Universitaria di Monserrato SS554, 09042 Monserrato, Italy*

[d]*Department of Clinical Nutrition, College of Applied Health Sciences, Qassim University, Ar Rass 51921, Saudi Arabia*

[e]*Laboratoire de Caractérisations, Applications et Modélisations des Matériaux, Faculté des Sciences de Tunis, Université Tunis El Manar, Tunis, Tunisia*

[f]*Department of Chemistry, College of Science and Arts at Ar Rass, Qassim University, P.O. Box 53, Ar Rass 51921, Saudi Arabia*

[g]*University Mohamed Khider, Department of Matter Sciences, BP 145 RP, Biskra, Algeria*

[h]*Laboratory of Natural and Bio-active Substances, Faculty of Science, Tlemcen University, P.O. Box 119, Tlemcen, Algeria*

[i]*Organische Chemie I, Universität Bayreuth, Universitätsstrasse 30, 95447 Bayreuth, Germany*

[*]Corresponding author.

E-mail addresses:

bernhard.biersack@uni-bayreuth.de, bernhard.biersack@yahoo.com (Bernhard Biersack)

ABSTRACT

A series of 1*H*-indeno[2',1':5,6]dihydropyrido[2,3-*d*]pyrimidine and 1*H*-indeno[2',1':5,6]pyrido[2,3-*d*]pyrimidine derivatives was prepared and screened for antiparasitic and viral RNase H inhibitory activity. Several compounds showed considerable activity against *Toxoplasma gondii* parasites and *Leishmania major* amastigotes, which warrants further investigation. Based on the structural similarities of certain derivatives with common viral RNase H inhibitors, a HIV-1 RNase H assay was used to study the RNase H inhibition by selected test compounds. Docking of active derivatives into the active site of the HIV-1 RNase H enzyme was carried out. The new compound **2a**, inactive in the antiparasitic tests, showed distinct HIV-1 RNase H inhibition. Thus, ring substitution determines antiparasitic or HIV-1 RNase H inhibitory activity of this promising compound class.

*Keywords***:** Pyrimidine; multi-component reaction; Antiviral drugs; Antiparasitic drugs; HIV-1 RNase H

1. Introduction

Infectious diseases can be harmful and even lethal ailments posing a considerable threat to humans.[1] Some tropical infectious diseases belong to the class of neglected tropical diseases (NTDs), where proper treatments are unavailable, toxic, and/or too expensive for patients in tropical regions.[2] In addition, viral infections can quickly spread to form worldwide epidemics with considerable danger to health and economic systems.[3]

Leishmaniasis is classified as an NTD and clinically subdivided into visceral leishmaniasis (VL), cutaneous leishmaniasis (CL), and mucocutaneous leishmaniasis (MCL), affecting vast regions from South and Central America over Africa to Asia. The CL form brought about by various *Leishmania* species such as *L. major*, *L. tropica*, *L. mexicana*, *L. amazonensis* etc., causes severe skin lesions. It is the most prevalent leishmaniasis form responsible for up to 1 million, mostly young, patients annually.[4,5] Although usually not lethal, CL leads to stark and disfiguring skin lesions and to stigmatization of affected persons.[6,7] CL patients are currently treated with pentavalent antimonials, miltefosine, amphotericin or pentamidine.[5] Aside from the general toxicity of clinically applied drugs such as antimonials, another growing problem is the emergence of drug-resistant parasite forms. Thus, new potent anti-parasitic drugs against leishmaniasis are needed. As immune-compromised people risk severe complications when infected with the globally occurring *Toxoplasma gondii* parasites (i.e., the causative agents of toxoplasmosis), new drugs for the treatment of toxoplasmosis in such patients are necessary.[8]

About 35 million people have globally died of the acquired immunodeficiency syndrome (AIDS) since the 1980's (www.unaids.com). AIDS is a consequence of an infection with the human immunodeficiency virus type 1 and type 2 (HIV-1 and HIV-2), and ca. 38.4 million people including ca. 1.7 million children under 15 were infected in 2021 worldwide leading to 650.000 annual AIDS-related deaths (www.unaids.com). There is neither cure of nor vaccine for HIV, and the latent infection of tissue reservoirs make it difficult to cure the disease.[9,10] Highly active antiretroviral therapy (HAART) based on a cocktail of HIV protease inhibitors, HIV reverse transcriptase (RT, inhibition of its DNA polymerase subunit RDDP/RNA-dependent DNA polymerase) inhibitors, and inhibitors of HIV integrase (IN), is currently applied for the treatment of HIV aiming at a suppression of HIV replication and the prevention of an outbreak of AIDS. However, treatment with these antiviral drugs often leads to notable side-effects and drug resistance.[11–13] In addition, HIV patients, who are co-infected with other

harmful diseases such as hepatitis B (HBV) or leishmaniasis, are experiencing considerable health issues especially in under-developed countries.[14,15]

In order to overcome HIV resistance to the treatment with RT inhibitors, new targets must be identified and investigated. In addition to a DNA polymerase domain, the HIV-1 RT enzyme also has an RNase H domain, which degrades unspecifically the RNA of RNA/DNA intermediates, but also catalyzes specifically the hydrolysis of RNA primers of integration-competent pro-viral DNA precursors.[16] The active site of the HIV-1 RT-associated RNase H is formed by the DEDD motif of four conserved negatively charged amino acids coordinating two Mg^{2+} ions required for phosphate ester hydrolysis in RNA molecules. These Mg^{2+} ions can be exchanged by Mn^{2+} without loss of enzymatic activity.[17,18] In terms of possible new drugs against HIV, several HIV-1 RNase H inhibitors were investigated meanwhile. While competitive active site inhibitors of HIV-1 (and of HBV) RNase H coordinate the active site Mg^{2+} ions, allosteric inhibitors destabilize the protein.[19] In addition to synthetic inhibitors, various natural products were found active against HIV-1 RNase H, too.[20–22] The great potential of RNase H inhibitors is corroborated by the fact, that the HIV-1 RT-associated RNase H domain is highly conserved among naïve and drug-experienced patients as well as by the recently observed breach of RT resistance upon inhibition of HIV-1 RNase H.[23,24]

Considering the critical health care situation in poor countries and the emergence of drug resistance, new cost-effective drugs and treatment options for viral and protozoal infectious diseases are needed (www.dndi.org). Multicomponent reactions are a useful, atom-economic and cost-effective tool for synthesizing new anti-infective drug candidates.[25] The fusion of 6-aminouracil with indan-1,3-dione and an aryl aldehyde led to the formation of anticancer active 1*H*-indeno[2,1:5,6]dihydropyrido[2,3-*d*]pyrimidines such as compounds **1a** and **1b** (Figure 1). Subsequent oxidation to the corresponding pyrimidines **1c** and **1d** generated topoisomerase II inhibitors indicating that **1a** and **1b** can be considered as prodrugs of such topoisomerase II

inhibitors, which can be activated by intracellular oxidation.[26] Some of these compounds published before were repurposed for anti-infective testing in the present work. In addition, by modification of the aryl aldehyde component, several new antiparasitic compounds and/or HIV1 RT-associated RNase H inhibitors were identified in this study.

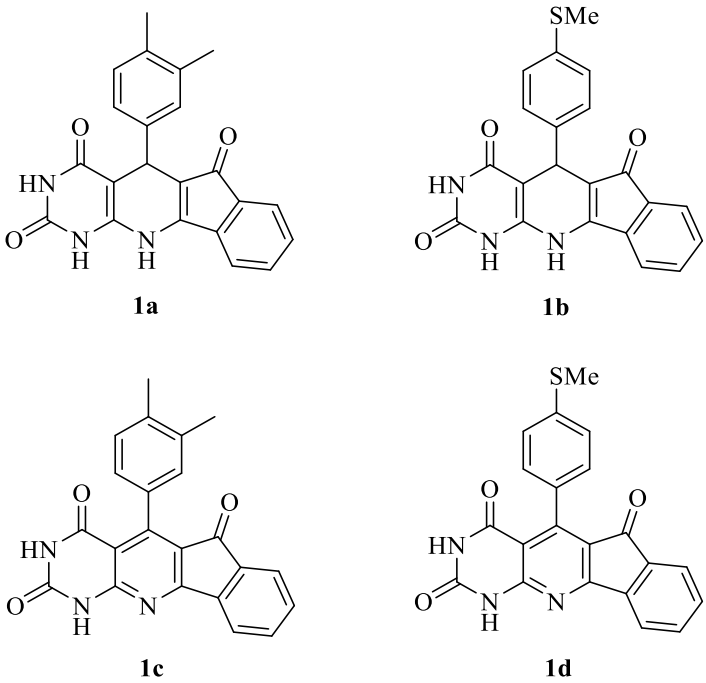

Fig. 1. Structures of anticancer active pyrimidines **1a–d**.

2. Materials and Methods

2.1. Chemistry

Starting compounds and reagents were purchased from Aldrich, Alfa Aesar, and TCI. The known compounds **2b**, **2c**, **2e-g**, **2n**, **3e**, and **3n** were prepared according to literature procedures, analyzed, and found identical to published data.[26,27]

2.1.1. Synthesis of test compounds

5-(3,4-Dihydroxyphenyl)-5,11-dihydro-1H-indeno[2',1':5,6]pyrido[2,3-d]pyrimidine-2,4,6(3H)-trione 2a

Indan-1,3-dione (117 mg, 0.8 mmol), 6-aminouracil (97 mg, 0.76 mmol) and 3,4-dihydroxybenzaldehyde (110 mg, 0.8 mmol) were suspended in AcOH / ethylene glycol (6 mL, 2:1). The reaction mixture was stirred at 120 °C for 4 h. After cooling to room temperature, the formed precipitate was collected and washed with ethanol. Yield: 120 mg (0.32 mmol, 42%); red solid of mp >340 °C (dec.); υ_{max}(ATR)/cm^{-1} 3548, 3320, 3281, 3063, 2879, 1712, 1687, 1661, 1644, 1607, 1517, 1442, 1392, 1367, 1347, 1261, 1247, 1206, 1169, 1139, 1111, 1073, 1022, 977, 941, 907, 872, 823, 789, 762, 749, 730, 714, 702, 669, 655, 636, 611; ^{1}H NMR (300 MHz, DMSO-d$_6$) δ 4.50 (1 H, s), 6.4-6.6 (2 H, m), 6.64 (1 H, s), 7.2-7.5 (4 H, m), 8.56 (1 H, s), 8.70 (1 H, s), 10.06 (1 H, s), 10.27 (1 H, s), 10.88 (1 H, s); ^{13}C NMR (75.5 MHz, DMSO-d$_6$) δ 32.4, 91.4, 110.2, 115.1, 118.3, 118.8, 120.7, 130.2, 132.1, 132.6, 135.9, 136.4, 143.7, 144.2, 144.6, 149.8, 153.0, 162.8, 190.9; *m/z* (%) 265 (100), 222 (62), 110 (51).

5-(3-Hydroxy-4-methoxyphenyl)-5,11-dihydro-1H-indeno[2',1':5,6]pyrido[2,3-d]pyrimidine-2,4,6(3H)-trione 2d

Analogously to the synthesis of **2a**, compound **2d** was obtained from indan-1,3-dione (117 mg, 0.8 mmol), 6-aminouracil (97 mg, 0.76 mmol) and isovanillin (122 mg, 0.8 mmol) in AcOH / ethylene glycol (6 mL, 2:1). Yield: 126 mg (0.32 mmol, 42%); orange solid of mp 294-295 °C; υ_{max}(ATR)/cm^{-1} 3519, 3324, 3260, 3225, 3203, 3105, 2940, 2810, 1716, 1689, 1655, 1620, 1500, 1456, 1428, 1381, 1371, 1358, 1321, 1274, 1255, 1210, 1174, 1148, 1120, 1074, 1015, 981, 941, 911, 880, 822, 787, 764, 750, 709, 695, 678, 643, 623, 608; ^{1}H NMR (300 MHz, DMSO-d$_6$) δ 3.67 (3 H, s), 4.53 (1 H, s), 6.6-6.8 (3 H, m), 7.2-7.5 (4 H, m), 8.81 (1 H, s), 10.0-10.3 (2 H, m), 10.92 (1 H, s); ^{13}C NMR (75.5 MHz, DMSO-d$_6$) δ 32.6, 55.7, 91.3, 110.0, 112.1,

115.1, 118.2, 118.9, 120.8, 130.3, 132.1, 132.6, 135.9, 138.1, 144.3, 146.1, 149.9, 153.1, 162.8, 190.9; *m/z* (%) 389 (74) [M^+], 358 (27), 266 (100), 223 (53).

5-(4-Methoxy-3-methylphenyl)-5,11-dihydro-1H-indeno[2',1':5,6]pyrido[2,3-d]pyrimidine-2,4,6(3H)-trione 2h

Analogously to the synthesis of **2a**, compound **2h** was obtained from indan-1,3-dione (117 mg, 0.8 mmol), 6-aminouracil (97 mg, 0.76 mmol) and 3-methyl-4-methoxybenzaldehyde (120 mg, 0.8 mmol) in AcOH / ethylene glycol (6 mL, 2:1). The reaction mixture was stirred at 120 °C for 4 h. Yield: 126 mg (0.33 mmol, 43%); orange solid of mp 318-319 °C; υ_{max}(ATR)/cm^{-1} 3209, 3112, 2948, 2832, 1736, 1688, 1662, 1637, 1601, 1533, 1493, 1455, 1439, 1388, 1362, 1346, 1322, 1295, 1256, 1210, 1170, 1143, 1130, 1075, 1036, 1008, 941, 913, 816, 800, 788, 743, 718, 702, 665, 609; ^{1}H NMR (300 MHz, DMSO-d_6) δ 2.06 (3 H, s), 3.70 (3 H, s), 4.58 (1 H, s), 6.9-7.0 (2 H, m), 7.2-7.5 (4 H, m), 10.0-10.3 (2 H, m), 10.88 (1 H, s); ^{13}C NMR (75.5 MHz, DMSO-d_6) δ 16.1, 32.6, 55.1, 91.3, 109.8, 110.0, 118.9, 120.7, 124.7, 126.0, 129.5, 130.3, 132.1, 132.6, 135.9, 137.0, 144.3, 149.8, 153.1, 155.8, 162.8, 190.9; *m/z* (%) 387 (93) [M^+], 356 (43), 266 (100), 223 (52).

5-(3-Bromo-4-methoxyphenyl)-5,11-dihydro-1H-indeno[2',1':5,6]pyrido[2,3-d]pyrimidine-2,4,6(3H)-trione 2i

Analogously to the synthesis of **2a**, compound **2i** was obtained from indan-1,3-dione (117 mg, 0.8 mmol), 6-aminouracil (97 mg, 0.76 mmol) and 3-bromo-4-methoxybenzaldehyde (172 mg, 0.8 mmol) in AcOH / ethylene glycol (6 mL, 2:1). Yield: 133 mg (0.29 mmol, 38%); orange solid of mp 316-318 °C; υ_{max}(ATR)/cm^{-1} 3243, 3205, 3099, 2842, 1738, 1688, 1662, 1638, 1602, 1533, 1494, 1456, 1438, 1387, 1285, 1259, 1215, 1169, 1142, 1075, 1053, 1022, 914, 788, 765, 743, 709, 637, 625, 606; ^{1}H NMR (300 MHz, DMSO-d_6) δ 3.77 (3 H, s), 4.62 (1 H, s), 6.97 (1 H, d, J = 8.6 Hz), 7.20 (1 H, d, J = 8.6 Hz), 7.3-7.5 (5 H, m), 10.1-10.4 (2 H, m),

10.95 (1 H, s); ^{13}C NMR (75.5 MHz, DMSO-d$_6$) δ 32.7, 56.1, 90.7, 110.0, 112.3, 119.1, 120.9, 128.1, 130.4, 131.8, 132.2, 135.7, 139.0, 144.6, 149.8, 153.4, 153.8, 162.8, 190.8; *m/z* (%) 451 (83) [M$^+$], 424 (10), 422 (15), 372 (45). 266 (100), 233 (75).

5-(3-Bromophenyl)-5,11-dihydro-1H-indeno[2',1':5,6]pyrido[2,3-d]pyrimidine-2,4,6(3H)-trione 2j

Analogously to the synthesis of **2a**, compound **2j** was obtained from indan-1,3-dione (117 mg, 0.8 mmol), 6-aminouracil (97 mg, 0.76 mmol) and 3-bromobenzaldehyde (148 mg, 0.8 mmol) in AcOH / ethylene glycol (6 mL, 2:1). Yield: 114 mg (0.27 mmol, 36%); orange solid of mp >290 °C (dec.); υ_{max}(ATR)/cm^{-1} 3357, 3130, 1705, 1657, 1615, 1589, 1517, 1456, 1396, 1357, 1283, 1162, 1086, 1025, 849, 805, 781, 763; ^{1}H NMR (300 MHz, DMSO-d$_6$) δ 5.31 (1 H, s), 6.6-6.8 (3 H, m), 7.0-7.5 (5 H, m), 10.34 (2 H, s), 10.54 (1 H, s); ^{13}C NMR (75.5 MHz, DMSO-d$_6$) δ 32.4, 90.3, 108.8, 119.2, 120.9, 121.3, 125.8, 126.8, 127.9, 129.2, 129.8, 130.3, 130.5, 132.5, 135.7, 142.8, 147.8, 149.7, 153.7, 162.8, 190.7; HRMS for $C_{20}H_{13}O_3N_3Br$ [M$^+$ + H] calcd. 422.01348, found 422.01291.

5-(3-Fluoro-4-methoxyphenyl)-5,11-dihydro-1H-indeno[2',1':5,6]pyrido[2,3-d]pyrimidine-2,4,6(3H)-trione 2k

Analogously to the synthesis of **2a**, compound **2k** was obtained from indan-1,3-dione (117 mg, 0.8 mmol), 6-aminouracil (97 mg, 0.76 mmol) and 3-fluoro-4-methoxybenzaldehyde (123 mg, 0.8 mmol) in AcOH / ethylene glycol (6 mL, 2:1). Yield: 140 mg (0.36 mmol, 47%); orange solid of mp >270 °C (dec.); υ_{max}(ATR)/cm^{-1} 3163, 3062, 1742, 1708, 1665, 1642, 1604, 1537, 1516, 1497, 1442, 1388, 1322, 1272, 1214, 1172, 1141, 1116, 1076, 1027, 978, 938, 908, 849, 824, 788, 760, 745, 722, 703, 689, 667; ^{1}H NMR (300 MHz, DMSO-d$_6$) δ 4.63 (1 H, s), 7.0-7.1 (3 H, m), 7.3-7.5 (4 H, m), 10.1-10.4 (2 H, m), 10.92 (1 H, s); ^{13}C NMR (75.5 MHz, DMSO-d$_6$) δ 32.5, 55.9, 90.7, 109.2, 113.4, 115.0-115.2 (m), 119.1, 120.9, 123.5, 130.4, 132.2, 132.5,

135.8, 144.6, 145.4-145.5 (m), 149.5, 149.8, 152.7, 153.4, 162.9, 190.9; HRMS for $C_{21}H_{15}O_4N_3F$ [M^+ + H] calcd. 392.10411, found 392.10351.

5-(3,4,5-Trimethoxyphenyl)-5,11-dihydro-1H-indeno[2',1':5,6]pyrido[2,3-d]pyrimidine-2,4,6(3H)-trione 2l

Analogously to the synthesis of **2a**, compound **2l** was obtained from indan-1,3-dione (117 mg, 0.8 mmol), 6-aminouracil (97 mg, 0.76 mmol) and 3,4,5-trimethoxybenzaldehyde (157 mg, 0.8 mmol) in AcOH / ethylene glycol (6 mL, 2:1). Yield: 155 mg (0.36 mmol, 47%); pale-brown solid of mp 339-340 °C; υ_{max}(ATR)/cm^{-1} 3349, 3269, 3196, 3122, 2959, 2825, 1719, 1694, 1661, 1627, 1600, 1585, 1524, 1493, 1455, 1427, 1415, 1390, 1368, 1350, 1328, 1317, 1296, 1235, 1213, 1202, 1189, 1169, 1138, 1128, 1094, 1076, 1028, 1003, 979, 952, 909, 895, 858, 842, 817, 801, 774, 766, 756, 732, 717, 700, 658, 651, 627, 607; ^{1}H NMR (300 MHz, DMSO-d_6) δ 3.59 (3 H, s), 3.70 (6 H, s), 4.67 (1 H, s), 6.53 (2 H, s), 7.3-7.5 (4 H, m), 10.1-10.3 (2 H, m), 10.94 (1 H, s); ^{13}C NMR (75.5 MHz, DMSO-d_6) δ 33.7, 55.8, 59.8, 90.5, 105.0, 109.3, 119.0, 120.9, 130.3, 132.1, 132.6, 135.8, 136.1, 140.6, 144.8, 149.8, 152.5, 153.4, 162.9, 190.9; *m/z* (%) 433 (100) [M^+], 402 (83), 359 (21), 266 (53), 223 (32).

5-(3-Chloro-4,5-dimethoxyphenyl)-5,11-dihydro-1H-indeno[2',1':5,6]pyrido[2,3-d]pyrimidine-2,4,6(3H)-trione 2m

Analogously to the synthesis of **2a**, compound **2m** was obtained from indan-1,3-dione (117 mg, 0.8 mmol), 6-aminouracil (97 mg, 0.76 mmol) and 3-chloro-4,5-dimethoxybenzaldehyde (160 mg, 0.8 mmol) in AcOH / ethylene glycol (6 mL, 2:1). Yield: 122 mg (0.28 mmol, 37%); orange solid of mp 340-341 °C; υ_{max}(ATR)/cm^{-1} 3343, 3274, 3205, 3126, 2966, 2828, 1721, 1698, 1663, 1627, 1572, 1524, 1489, 1453, 1417, 1393, 1368, 1351, 1314, 1279, 1261, 1231, 1198, 1169, 1138, 1075, 1050, 997, 982, 951, 909, 892, 855, 812, 801, 788, 764, 750, 743, 729, 716, 697, 653; ^{1}H NMR (300 MHz, DMSO-d_6) δ 3.68 (3 H, s), 3.79 (3 H, s), 4.68 (1 H, s), 6.78 (1 H, s), 6.97 (1 H, s), 7.2-7.5 (4 H, m), 10.1-10.4 (2 H, m), 10.96 (1 H, s); ^{13}C NMR (75.5 MHz,

DMSO-d_6) δ 33.5, 56.0, 60.0, 90.1, 108.7, 111.7, 119.1, 119.8, 120.9, 126.4, 130.5, 132.2, 132.5, 135.7, 141.9, 143.0, 144.9, 149.8, 153.0, 153.6, 162.9, 190.8; *m/z* (%) 437 (57) [M^+], 402 (35), 266 (100), 223 (52).

5-(3-Iodo-4,5-dimethoxyphenyl)-5,11-dihydro-1H-indeno[2',1':5,6]pyrido[2,3-d]pyrimidine-2,4,6(3H)-trione 2o

Analogously to the synthesis of **2a**, compound **2o** was obtained from iIndan-1,3-dione (117 mg, 0.8 mmol), 6-aminouracil (97 mg, 0.76 mmol) and 3-iodo-4,5-dimethoxybenzaldehyde (234 mg, 0.8 mmol) in AcOH / ethylene glycol (6 mL, 2:1). Yield: 147 mg (0.28 mmol, 37%); orange solid of mp 333-335 °C; υ_{max}(ATR)/cm^{-1} 3198, 3056, 3009, 2933, 2868, 2788, 1713, 1693, 1662, 1639, 1607, 1586, 1537, 1496, 1480, 1448, 1425, 1407, 1388, 1361, 1313, 1274, 1254, 1237, 1218, 1174, 1145, 1075, 1040, 1001, 940, 913, 852, 829, 806, 788, 764, 738, 727, 708, 688, 652; ^{1}H NMR (300 MHz, DMSO-d_6) δ 3.64 (3 H, s), 3.77 (6 H, s), 4.65 (1 H, s), 6.99 (1 H, s), 7.08 (1 H, s), 7.3-7.5 (4 H, m), 10.1-10.4 (2 H, m), 10.95 (1 H, s); ^{13}C NMR (75.5 MHz, DMSO-d_6) δ 33.7, 55.8, 59.7, 90.2, 92.3, 108.8, 113.3, 119.2, 120.9, 128.3, 130.5, 132.2, 132.5, 135.7, 143.2, 144.8, 146.6, 149.8, 151.8, 153.6, 162.8, 190.8; *m/z* (%) 529 (63) [M^+], 402 (31), 266 (100), 223 (52), 44 (30).

5-(3-Bromo-4-methoxyphenyl)-1H-indeno[2',1':5,6]pyrido[2,3-d]pyrimidine-2,4,6(3H)-trione 3i

2i (37 mg, 0.082 mmol) was dissolved in hot DMF (1 mL) and *p*-chloranil (21 mg, 0.085 mmol) was added. The reaction mixture was stirred at 120 °C for 5 min. H_2O (0.1 mL) was added and the reaction mixture was stirred at 120 °C for 3 min. After cooling to room temperature, the formed precipitate was collected and washed with ethanol. Yield: 34 mg (0.076 mmol, 93%); yellow solid of mp >290 °C (dec.); υ_{max}(ATR)/cm^{-1} 3167, 3056, 2841, 1713, 1642, 1567, 1497, 1396, 1365, 1288, 1255, 1204, 1185, 1133, 1055, 1021, 1000, 942, 872, 830, 816, 797, 782,

749, 717, 692, 673; ^{1}H NMR (300 MHz, DMSO-d$_6$) δ 3.92 (3 H, s), 7.11 (1 H, d, J = 8.6 Hz), 7.27 (1 H, d, J = 8.6 Hz), 7.51 (1 H, s), 7.6-7.7 (2 H, m), 7.7-7.9 (2 H, m), 7.95 (1 H, s), 11.33 (1 H, s), 12.22 (1 H, s); ^{13}C NMR (75.5 MHz, DMSO-d$_6$) δ 56.2, 106.8, 109.1, 111.1, 120.6, 121.5, 123.4, 127.4, 129.1, 132.5, 132.9, 140.1, 149.8, 155.1, 157.4, 161.2, 168.3, 188.2; HRMS for $C_{21}H_{13}O_4N_3Br$ [M^+ + H] calcd. 450.00839, found 450.00818.

5-(3-Fluoro-4-methoxyphenyl)-1H-indeno[2',1':5,6]pyrido[2,3-d]pyrimidine-2,4,6(3H)-trione 3k

Analogously to the synthesis of **3i**, compound **3k** was obtained from **2k** (32 mg, 0.082 mmol) and *p*-chloranil (21 mg, 0.085 mmol) in hot DMF (1 mL). Yield: 22 mg (0.057 mmol, 70%); yellow solid of mp 314 °C; υ_{max}(ATR)/cm^{-1} 3019, 2932, 1736, 1710, 1690, 1679, 1611, 1552, 1515, 1443, 1373, 1316, 1288, 1274, 1258, 1213, 1204, 1179, 1166, 1155, 1134, 1107, 1022, 1007, 951, 921, 905, 840, 826, 796, 770, 742, 713, 706, 686, 671; ^{1}H NMR (300 MHz, DMSO-d$_6$) δ 3.91 (3 H, s), 7.0-7.2 (3 H, m), 7.6-7.7 (2 H, m), 7.7-7.9 (2 H, m), 7.95 (1 H, s), 11.32 (1 H, s), 12.22 (1 H, s); ^{13}C NMR (75.5 MHz, DMSO-d$_6$) δ 55.9, 106.8, 112.3, 116.0-116.2 (m), 120.6, 121.5, 123.4, 124.7, 126.4-126.5 (m), 132.9, 135.4, 136.0, 139.5, 140.1, 146.8-146.9 (m), 148.9, 149.8, 150.1, 152.1, 157.4, 161.1, 168.2, 188.1; HRMS for $C_{21}H_{13}O_4N_3F$ [M^+ + H] calcd. 390.08846, found 390.08824.

5-(3,4,5-Trimethoxyphenyl)-1H-indeno[2',1':5,6]pyrido[2,3-d]pyrimidine-2,4,6(3H)-trione 3l

Analogously to the synthesis of **3i**, compound **3l** was obtained from **2l** (36 mg, 0.082 mmol) and *p*-chloranil (21 mg, 0.085 mmol) in hot DMF (1 mL). Yield: 35 mg (0.081 mmol, 99%); yellow solid of mp 357-359 °C; υ_{max}(ATR)/cm^{-1} 3179, 3086, 3004, 2966, 2928, 2890, 2840, 1705, 1582, 1556, 1522, 1507, 1454, 1428, 1414, 1403, 1369, 1329, 1304, 1274, 1256, 1245, 1230, 1168, 1151, 1124, 1047, 1026, 993, 962, 917, 839, 824, 776, 753, 737, 718, 705, 699, 690, 680, 647, 615; ^{1}H NMR (300 MHz, DMSO-d$_6$) δ 3.71 (6 H, s), 3.75 (3 H, s), 6.50 (2 H, s),

7.6-7.7 (2 H, m), 7.7-7.9 (2 H, m), 11.29 (1 H, s), 12.19 (1 H, s); ^{13}C NMR (75.5 MHz, DMSO-d_6) δ 55.9, 60.0, 105.7, 106.8, 120.6, 121.5, 123.4, 129.6, 132.9, 135.3, 136.0, 137.2, 140.1, 149.8, 151.6, 152.0, 157.3, 160.8, 168.2, 187.9; *m/z* (%) 431 (100) [M^+], 416 (33), 302 (25).

5-(3-Chloro-4,5-dimethoxyphenyl)-1H-indeno[2',1':5,6]pyrido[2,3-d]pyrimidine-2,4,6(3H)-trione 3m

Analogously to the synthesis of **3i**, compound **3m** was obtained from **2m** (36 mg, 0.082 mmol) and *p*-chloranil (21 mg, 0.085 mmol) in hot DMF (1 mL). Yield: 30 mg (0.069 mmol, 84%); yellow solid of mp 314-315 °C; υ_{max}(ATR)/cm^{-1} 3603, 3171, 3009, 2940, 2833, 1712, 1608, 1557, 1532, 1489, 1447, 1429, 1406, 1365, 1319, 1296, 1270, 1257, 1235, 1211, 1177, 1148, 1127, 1096, 1052, 1027, 1003, 958, 919, 864, 827, 817, 797, 744, 712, 694, 685, 667, 635, 612; ^{1}H NMR (300 MHz, DMSO-d_6) δ 3.76 (3 H, s), 3.84 (3 H, s), 6.95 (1 H, s), 6.99 (1 H, s), 7.6-7.9 (4 H, m), 11.35 (1 H, s), 12.25 (1 H, s); ^{13}C NMR (75.5 MHz, DMSO-d_6) δ 56.2, 60.2, 106.8, 112.1, 120.6, 120.7, 121.5, 123.5, 125.7, 130.9, 133.0, 135.4, 136.0, 140.1, 144.1, 149.6, 149.7, 152.5, 157.3, 160.9, 168.2, 188.0; *m/z* (%) 437 (33) [M^+], 435 (100) [M^+], 420 (22), 342 (27).

5-(3-Iodo-4,5-dimethoxyphenyl)-1H-indeno[2',1':5,6]pyrido[2,3-d]pyrimidine-2,4,6(3H)-trione 3o

Analogously to the synthesis of **3i**, compound **3o** was obtained from **2o** (43 mg, 0.082 mmol) and *p*-chloranil (21 mg, 0.085 mmol) in hot DMF (1 mL). Yield: 21 mg (0.040 mmol, 49%); yellow solid of mp 332-333 °C; υ_{max}(ATR)/cm^{-1} 3162, 3060, 2929, 2834, 1713, 1645, 1608, 1564, 1527, 1482, 1463, 1428, 1407, 1366, 1315, 1294, 1255, 1203, 1174, 1144, 1100, 1046, 1019, 1000, 952, 919, 822, 794, 776, 743, 681, 653, 632, 612; ^{1}H NMR (300 MHz, DMSO-d_6) δ 3.75 (3 H, s), 3.79 (3 H, s), 7.04 (1 H, s), 7.23 (1 H, s), 7.6-7.9 (4 H, m), 11.33 (1 H, s), 12.23 (1 H, s); ^{13}C NMR (75.5 MHz, DMSO-d_6) δ 56.0, 59.9, 91.0, 106.7, 113.7, 120.6, 121.5, 123.5,

128.9, 132.2, 132.9, 135.4, 136.0, 140.1, 147.7, 149.4, 149.8, 151.2, 157.4, 161.1, 168.2, 188.1; *m/z* (%) 527 (100) [M^+], 512 (14), 357 (17), 342 (22).

2.2. Antiparasitic activity and cytotoxicity assays

The investigations with the compounds conducted as described previously.[28] *T. gondii* tachyzoites (RH strain) that were obtained from Dr. Saeed El-Ashram (State Key Laboratory for Agrobiotechnology, China Agricultural University, Beijing, China) were grown in 96-well plates by using RPMI 1640 containing 10% fetal bovine serum (FBS). As host cells, Vero cells (ATCC® CCL81TM, USA) were employed. Different concentrations of the test compounds were added to determine their activity after 4 hours, with atovaquone (ATO) serving as a positive control. The following equation was used to determine cell viability under an inverted microscope:

Inhibition (%) = (1 - infected experimental cells/infected control cells) x 100.

L. major promastigotes that were isolated from a Saudi individual in February 2016 and *L. major* amastigotes that were isolated from infected BALB/c mice were cultured and used for antileishmanial assays as reported previously.[29,30] The King Saud University's Pharmaceutical College provided the BALB/c mice, which were maintained in accordance with the committee on research ethics' rules under permit number 20-03-20 from the Deanship of Scientific Research at Qassim University. In 96-well plates, both types of *L. major* amastigotes and promastigotes were grown using RPMI 1640 with 10% FBS. The host cells for growing amastigotes were mouse macrophage cells. Different concentrations of the test compounds were added to determine their activity after 4 hours, with amphotericin B (AmB) serving as a positive control. MTT (tetrazolium salt of 3-(4,5-dimethylthiazole-2-yl)-2,5-diphenyl tetrazolium bromide) was applied and analyzed spectrophotometry by ELISA reader (spectrophotometer) at 570 nm for the identification of viable parasites.

Vero cells were also grown and used for the MTT assays of the test compounds as mentioned before.[30,31] 96-well plates were utilized for a 3-day incubation period with cells at various doses in RPMI 1640 with 5% FBS to test the cytotoxicity of the compounds. Then, to evaluate cell toxicity, a colorimetric assay using spectrophotometer was employed at 540 nm (CC_{50}).

2.3. HIV-1 RDDP-independent RNase H inhibition assay

HIV-1 RT-associated RNase H inhibition assay was carried out as described previously.[32,33] All experiments were done in triplicate.

2.4. Computational procedures

2.4.1. DFT calculations

Density functional theory computations were performed using Gaussian 16 package.[34] Full geometry optimization was conducted employing Becke3 and Lee-Yang-Parr correlation (B3LYP) functional in conjunction with the atom-pairwise dispersion correction based on tight-binding partial charges (D3) coupled with the 6-311G(d, p) basis set.[35–37] These optimizations consider the influence of solvent water through the CPCM model.[38] Tautomerism increases the effectiveness of compound **2a** as an enzyme inhibitor by modifying its interaction with the active site. Tautomerization results from the exchange of hydrogen atoms between nitrogen and oxygen atoms of the uracil moiety (Figure 2).[39] Transition states refer to the hydrogen transfer between tautomeric forms via a 4-ring system (**TS23**, **TS45** and **TS16**) or torsional motion out of the plane (**TS34**).[40]

2.4.2. Molecular docking

Molecular Operating Environment (MOE) software was employed for molecular docking calculations, which followed the same protocol steps as in our previously published studies.[41–43] The following default parameters were used: Placement: Triangle Matcher; Rescoring 1: London dG. The London dG scoring function was employed to estimate the lowest score energy of the complex with the best ligand pose. We used the previously DFT/b3lyp/6-311g (d.p) optimized structure of the two major **2a** tautomers **IPU1** and **IPU2** as ligands for the MOE-docking. The database was created by converting the tautomers into the format .mdb. The crystal structure of the complex between the HIV-1 RNase H domain (PDB IDs: 3K2P) with the co-crystallized ligand β-thujaplicinol ($C_{10}H_{12}O_3$) was downloaded from the RCSB website (http://www.rcsb.org/pdb) (Table S1).[44] The ligand of 3K2P is β-thujaplicinol, **[**2,7-dihydroxy-4-(propan-2-yl)cyclohepta-2,4,6-trien-1-one]. The X-ray crystal of the HIV-1 RNase H domain (PDB ID: 3K2P) was simplified by removing water molecules, ions, cofactors, and co-crystal ligands from the PDB structure. The co-crystallized ligand β-thujaplicinol was redocked into the HIV-1 RNase H domain (PDB ID: 3K2P) using MOE software in order to validate the docking method.[41] The resulting pose was nearly perfectly superimposed with the native ligand with an RMSD value of 0.952, which is below 2 Å.[45] This value testifies the accuracy of this method. Finally, the protein structure 3K2P was used to investigate the interaction of the **2a** tautomers **IPU1** and **IPU2** with the HIV-1 RNase H domain.

2.4.3. Machine learning: ADME-T predictions and physiochemical property calculations

Various parameters of physicochemical properties such as TPSA, nROT, MW, LogP, number of hydrogen bond acceptors (nHA) and number of hydrogen bond donors (nHD) were calculated by using SwissADME (http://www.swissadme.ch/) online server in order to verify the drug-likeness rules according to Lipinski, Veber, and Ghose.[46,47]

The absorption (**Caco-2:** Colon adenocarcinoma**, HIA:** Human intestinal absorption), distribution (**PPB:** Protein plasma binding, **BBB:** Blood–brain barrier), metabolism (**CYP1A2 inhibitor**, **CYP2C19 inhibitor**, **CYP2D6 inhibitor**), excretion (renal OCT2 substrate**,** total clearance in mL/min/kg) and toxicity **(hERG:** human Ether-à-go-go-Related Gene and **AMES** toxicity) parameters were analyzed using the pkCSM server (http://biosig.unimelb.edu.au/pkcsm/prediction).[48]

3. Results and discussion

Compounds **2** were prepared from 6-aminouracil, indan-1,3-dione and the corresponding substituted benzaldehyde by a one-pot reaction in a mixture of hot acetic acid and ethylene glycol. Compounds **3** were subsequently prepared from the oxidation of the corresponding compounds **2** with *p*-chloranil (Scheme 1).[26] In this study, 14 new compounds **2a**, **2d**, **2h–m**, **2o**, **3i**, **3k–m**, and **3o** were obtained as colored solids, and analyzed by NMR, IR and MS techniques. In addition, eight known compounds **2b**, **2c**, **2e–g**, **2n**, **3e**, and **3n** were prepared for the following biological activity tests in order to round out this study on anti-infectives.[26,27]

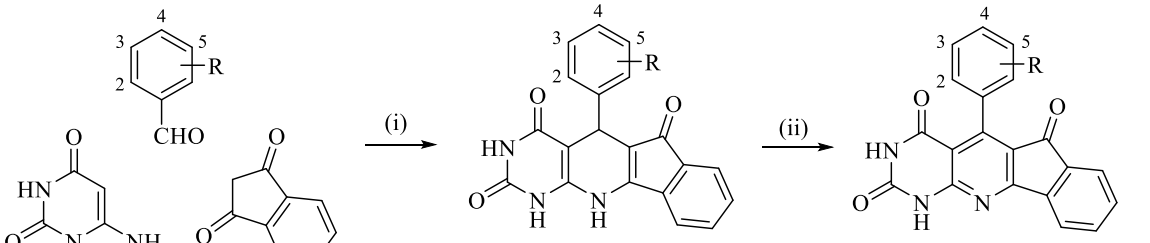

2a: R = 3,4-$(OH)_2$
2b: R = 4-OH, 3,5-$(OMe)_2$
2c: R = 3-OMe, 4-OH
2d: R = 3-OH, 4-OMe
2e: R = 3,4-$(OMe)_2$
2f: R = 3-OH
2g: R = 4-OH
2h: R = 3-Me, 4-OMe
2i: R = 3-Br, 4-OMe
2j: R = 3-Br
2k: R = 3-F, 4-OMe
2l: R = 3,4,5-$(OMe)_3$
2m: R = 3-Cl, 4,5-$(OMe)_2$
2n: R = 3-Br, 4,5-$(OMe)_2$
2o: R = 3-I, 4,5-$(OMe)_2$

3e: R = 3,4-$(OMe)_2$
3i: R = 3-Br, 4-OMe
3k: R = 3-F, 4-OMe
3l: R = 3,4,5-$(OMe)_3$
3m: R = 3-Cl, 4,5-$(OMe)_2$
3n: R = 3-Br, 4,5-$(OMe)_2$
3o: R = 3-I, 4,5-$(OMe)_2$

Scheme 1. Reagents and conditions: (i) AcOH/ethylene glycol (2:1), 120°C, 4 h, 36–47%; (ii)

p-chloranil, DMF, 120°C, 5 min, 49–99%.

The compounds were initially tested for their inhibition of *T. gondii* growth (Table 1). Compounds **2m–o** and **3m** showed high activities against *T. gondii* parasites with sub-micromolar IC_{50} values. **2i**, **3e**, and **3n** also showed considerable activity with IC_{50} values below 2.0 µM, followed by **2l**, **3l**, and **3o** with IC_{50} values of 2–3 µM. However, these compounds also exhibited high toxicity to non-malignant Vero cells indicating no or only slight selectivities for the *T. gondii* parasites. The lowest activities against *T. gondii* cells were observed for the hydroxyphenyl compounds **2f** and **2g** with IC_{50} values of 20.0 and 23.7 µM indicating a strong activity-reducing effect by mono-hydroxyphenyl substituents.

Table 1. Inhibitory cytotoxic concentrations CC_{50} (in µM) of test compounds when applied to cells of the Vero (African green monkey kidney epithelial) cell line, inhibitory concentrations IC_{50} when applied to cells of *Toxoplasma gondii*.[a] Atovaquone (ATO) was applied as positive control for the indicated cells.

Compd.	IC_{50} (*T. gondii*)	CC_{50} (Vero)	SI (Vero / *T. gondii*)[b]
2a	9.99	7.03	0.70
2b	10.97	6.08	0.55
2c	8.35	6.16	0.74
2d	11.43	8.99	0.79
2e	7.31	8.03	1.10
2f	23.7	9.46	0.40
2g	20.0	3.95	0.20
2h	9.81	2.89	0.30
2i	1.81	1.73	0.96
2j	11.37	16.1	1.42
2k	9.71	7.16	0.74
2l	2.77	2.10	0.76
2m	0.41	0.30	0.73
2n	0.73	0.50	0.69
2o	0.47	0.42	0.89
3e	1.12	0.87	0.78
3i	11.77	9.55	0.91

3k	9.25	4.11	0.44
3l	2.09	2.02	0.97
3m	0.69	0.85	1.23
3n	1.87	2.31	1.24
3o	2.47	2.22	0.90
ATO	0.07	9.5	136

[a]Values are the means of at least three independent experiments (SD ± 15%). They were obtained from concentration–response curves by calculating the percentage of treated cells in comparison to untreated controls after 72 h. [b]Selectivity index SI (CC_{50}/IC_{50}) was calculated from the corresponding CC_{50} values for the Vero cells and the IC_{50} values against *T. gondii*.

Compounds **2l–o** and **3l–o** have di- and trimethoxyphenyl substituents, which are also present in various tubulin binding anticancer agents, and might serve as an explanation for the relatively high activities and toxicities of these compounds.[49] The 3-chloro-4,5-dimethoxyphenyl derivatives **2m** and **3m** were distinctly more active than the analogous 3,4,5-trimethoxyphenyls **2l** and **3l**, thus, indicating a positive effect of chloro-substitution on anti-toxoplasmal activity in this compound series. 3-Bromo- and 3-iodo-3,4-dimethoxy substituents were only superior to 3,4,5-trimethoxyphenyl compounds among the compound **2** series (**2n** and **2o**) in terms of anti-toxoplasmal activity, and showed no advantages in series **3** compounds (**3m** and **3o**), which indicates that the oxidation state of the heterocyclic core of these compounds also contributes to activity against *T. gondii*. Such considerable activity differences were also observed for 3-bromo-4-methoxyphenyl compounds **2i** and **3i**, and it is noteworthy that **2i** showed virtually the same activity as **3n**.

In addition, the compounds were tested *in vitro* for their activity against *L. major* promastigotes and amastigotes (Table 2). Interestingly, several compounds were more active against amastigotes than against promastigotes, which is of clinical relevance since killing intramacrophageal amastigotes is a hallmark of potent antileishmanial drugs.[50] Compound **2i** was most active against the amastigotes with an IC_{50} of 1.9 µM, while it was inactive against the promastigotes (IC_{50} > 27.6 µM). Notably, the 3-bromo-4-methoxyphenyl derivative **2i** was distinctly active against *T. gondii*, too. Compounds **2e**, **2m**, **3e**, and **3l** also showed moderate

activities against the amastigotes with IC_{50} values of 5–7 µM, which were much higher than against promastigotes. In contrast to that, compounds **2k** and **3k** were more active against promastigotes than against amastigotes. Catechol **2a** was inactive against promastigotes and amastigotes.

Table 2. Inhibitory concentrations IC_{50} (in µM) of test compounds when applied to promastigotes and amastigotes of *Leishmania major*.[a] Amphotericin B (AmB) was applied as a positive control.

Compd.	IC_{50} promastigotes	IC_{50} amastigotes
2a	>33.3	>33.3
2b	31.7	21.2
2c	35.4	21.3
2d	>32.1	21.3
2e	>31.0	6.94
2f	>34.8	27.0
2g	>34.8	22.0
2h	>32.3	22.2
2i	>27.6	1.90
2j	11.6	36.5
2k	7.16	16.9
2l	>28.8	21.2
2m	>28.6	6.17
2n	>25.9	16.4
2o	>23.6	14.0
3e	29.4	6.73
3i	25.1	35.8
3k	6.68	15.7
3l	>29.0	5.80
3m	28.2	18.6
3n	26.0	16.2
3o	23.0	15.4
AmB	0.83	0.47

[a]Values are the means of three experiments (SD ± 15%). They were obtained from concentration–response curves by calculating the percentage of treated cells in comparison to untreated controls after 72 h.

Several catechol-based compounds exhibited inhibitory activity against HIV-1 RT-associated RNase H.[19,23,24,32] Hence, **2a** and its close analogs **2b–g** and **2l** were selected for the evaluation of their RNase H inhibitory activity (Table 3). Their activities were compared with the activity of the known HIV1-RNase H inhibitor RDS1759. **2a** showed considerable inhibition of the wild-type HIV1-RNase H (IC_{50} = 11.2 µM), which was only slightly lower than the activity of the positive control RDS1759 (IC_{50} = 8.7 µM). Moderate inhibitory activities were observed for **2b** (IC_{50} = 17.08 µM), **2e** (IC_{50} = 20.27 µM) and **2l** (IC_{50} = 21.50 µM). **2c**, **2d**, **2f** and **2g** showed no RNase H inhibitory activity. Aside the dihydroxyphenyl motif of **2a**, di-and trimethoxyphenyl motifs (**2b**, **2e**, **2l**) led to moderate RNase H inhibition, while (iso)vanillyl- (**2c**, **2d**) and mono-hydroxyphenyl scaffolds (**2f**, **2g**) had no RNase H inhibitory activity.

Table 3. Inhibitory concentrations IC_{50} (in µM)[a] of test compounds when tested against HIV-1 RT-associated RNase H activity of wildtype RTs. RDS1759 was applied as positive control.

Compound	HIV-1 RT RNase H
2a	11.2 ± 1.6
2b	17.08 ± 0.8
2c	>100
2d	>100
2e	20.27 ± 2.8
2f	93.43 ± 11.8
2g	>100
2l	21.50 ± 7.2
RDS1759	8.7 ± 3.1

[a]Compound concentration required to reduce the HIV-1 RT-associated RNase H activity by 50%

In order to investigate the HIV-1 RNase H binding mode of **2a**, docking calculations were performed. Detailed results of the docking calculations and the best poses received after docking of the **2a**-tautomers **IPU1** and **IPU2** (Figures 2 and S1) and the known ligand β-thujaplicinol with the HIV RNase H domain (PDB ID: 3K2P) are summarized in Table 4. The docking outputs generated by MOE software were converted into (.pdb) files and visualized

with the default parameters of the *BIOVIA DS* visualizer package (*Dassault Systèmes BIOVIA, Discovery Studio Modeling Environment*, 2020) to estimate all possible bonds.

Table 4. S-score (binding energy in kcal mol^{-1}) and interactions between **2a**-tautomers **IPU1** and **IPU2** and the active site residues of the HIV-1 RNase H domain (PDB ID: 3K2P).

Tautomers of 2a	Score (kcal mol^{-1})	Bonds between atoms of compounds and active site residues					
		Atom of compound	Involved receptor atoms	Involved receptor residues	Category	Type of interaction/ bond	Distance (Å)
IPU1	-3.531	O	HE21	GLN475(A)	Hydrogen bond	Conventional H-bond	2.41
		H	OG	SER499(A)	Hydrogen bond	Conventional H-bond	2.32
		O	MN	MN901(A)	Other	Metal-Acceptor	1.89
		/	MN	MN901(A)	Electrostatic	Pi-Cation	4.73
		/	/	ALA538(A)	Hydrophobic	Pi-Alkyl	4.06
		/	/	ALA538(A)	Hydrophobic	Pi-Alkyl	4.19
IPU2	-1.954	H	OD1	ASP498(A)	Hydrogen bond	Conventional H-bond	2.98
		H	O	ALA446(A)	Hydrogen bond	Conventional H-bond	2.60
		H	OD1	ASN474(A)	Hydrogen bond	Conventional H-bond	2.91
		O	MN	MN901(A)	Other	Metal-Acceptor	1.92
		/	HD21	ASN474(A)	Hydrogen bond	Pi-Donor H-bond	2.55
		/	/	ALA538(A)	Hydrophobic	Pi-Alkyl	4.12
β-Thujaplicinol	-10.327	H2	NE2	HIS539(A)	Hydrogen bond	Conventional H-bond	1.85
		O1	MN	MN901(A)	Other	Metal-Acceptor	1.79
		O7	MN	MN901(A)	Other	Metal-Acceptor	1.32
RDS1759	-8.514	O	HH21	ARG557(A)	Hydrogen bond	Conventional H-bond	3.09
		H	OD1	ASP498(A)	Hydrogen bond	Conventional H-bond	2.36
		H	OD1	ASN474(A)	Hydrogen bond	Carbon H-bond	2.90
		H	O	ASP498(A)	Hydrogen bond	Carbon H-bond	3.00
		O1	MN	MN901(A)	Other	Metal-Acceptor	2.83
		O1	MN	MN901(A)	Other	Metal-Acceptor	2.03
		O1	MN	MN902(A)	Other	Metal-Acceptor	1.92
		/	NH2	ARG557(A)	Electrostatic	Pi-Cation	3.27
		/	HD21	ASN474(A)	Hydrogen bond	Pi-Donor H-bond	2.78
		C	/	ALA538(A)	Hydrophobic	Alkyl	4.00
		/	/	ALA445(A)	Hydrophobic	Pi-Alkyl	5.13

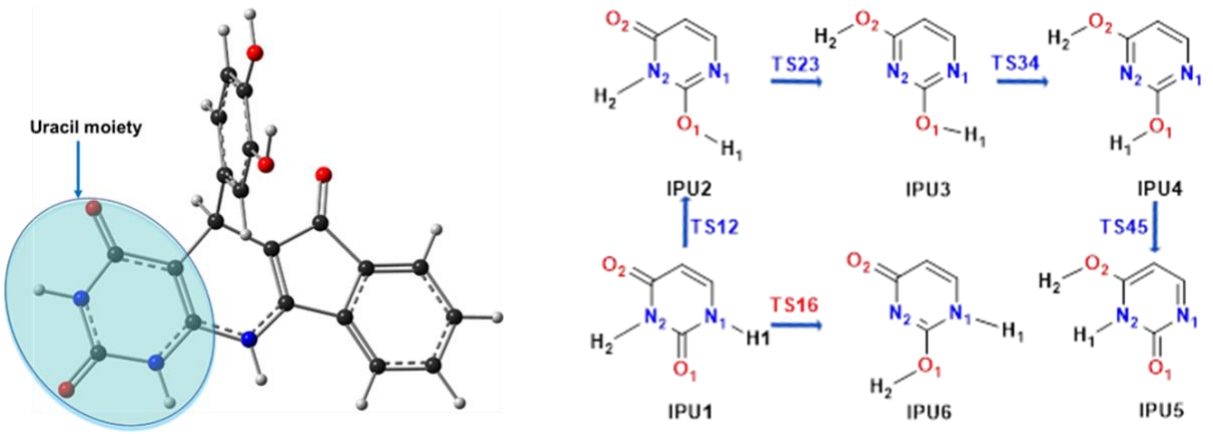

Fig. 2. Optimized geometry (left) and schematic representation of the tautomerisation of **2a** (**IPU1-6**, right).

Hydrogen transfer gives six tautomers, the di-keto form (**IPU1**), the keto-enol tautomers (**IPU2**, **IPU5** and **IPU6**), and the di-enol tautomers (**IPU3** and **IPU4**). Moreover, transition states were localized and denoted as TSXY (X and Y refer to the correlated tautomer numbers, e.g., **TS16**, **TS23**, **TS34**, **TS45**), which can be found in the Supporting Information (Figure S1, supporting information). The five isomers are stable (no imaginary frequency) and there is only one negative frequency for each transition state. The optimized geometries of five tautomers, the corresponding transition states and the relative free energies (ΔG^0 in kcal mol^{-1}) are given in Figure S1 concerning in relation to the most stable isomer **IPU1** tautomer (di-keto form), which functions as a reference. ΔG^0 values of the tautomers **IUP2-IPU6** were 7.80, 12.8, 12.81, 13.45 and 18.05 kcal mol^{-1}, respectively. Note that the energy differences among these five tautomers are nearly 18 kcal mol^{-1}. Therefore, the intramolecular interconversion barriers are evaluated. The interconversion between IPU3 and IPU4 results from the rotation of the O1H1 band, and the barrier between both rotamers is ca. 8 kcal mol^{-1}. Except for **TS34**, all barrier energies are greater than 40 kcal mol^{-1}. The two most stable tautomers **IPU1** and **IPU2** were used for molecular docking and ADME-T calculations.

The molecular docking results show that the score of binding (S-score) of both compounds were -3.531 and -1.954 kcal mol^{-1}, respectively, while the S-score of the β-thujaplicinol was -10.327 kcal mol^{-1} (Table 4). Both compounds established various types of interaction including H-bonds, metal-acceptor, and π-donor/alkyl interactions. Previous studies confirmed that similar types of binding are responsible for the formation of the binding complex in the active site, in particular, the interaction of β-thujaplicinol with the Mn^{2+} ion, which plays an essential role in the functioning of the enzyme.[17,18,51]

Both **2a**-tautomers **IPU1** and **IPU2** established six interactions with the pocket of the HIV-1 RNase H domain (Table 4 and Figure 3). Two strong hydrogen bonds were formed between tautomer **IPU1** and GLN475(A) and SER499(A) at distances of 2.41 and 2.32 Å, respectively, while IPU1 was also involved in two hydrophobic contacts with ALA538.[24,52,53] In addition, tautomer **IPU1** formed two bonds with the manganese ion (Mn^{+2}) of the active site, the first one is chelating the metal ion according to the metal-acceptor bond type (distance of 1.89 Å), the second one is of the π-cation type (distance of 4.73Å) (Table 4 and Figure 3a).

The second tautomer of **2a**, **IPU2**, established four strong H-bonds with the active site of the HIV-1 RNase H domain (PDB ID: 3K2P), three conventional H-bonds formed between **IPU2** and the ASP498(A), ALA446(A) and ASN474(A) at distances of 2.98, 2.60 and 2.91 Å, respectively. The fourth one is a strong π-donor type H-bond, which is formed between **IPU2** and ASN474(A) with a distance of 2.55 Å. In addition, one hydrophobic interaction appeared with ALA538(A) (Table 4 and Figure 3b), which is a binding mode described before by Zhang and coworkers.[54] The binding affinity of both tautomers of **2a** was lower than for β-thujaplicinol, which gave the lowest score energy of -10.327 kcal mol^{-1}. β-Thujaplicinol established three interactions with the binding pocket of the HIV-1 RNase H domain (PDB ID: 3K2P) receptor, among them one strong conventional H-bond formed between the native ligand and HIS539(A) with a distance of1.85 Å.[52] β-Thujaplicinol also coordinated the manganese ion

(Mn^{+2}) by forming two metal-acceptor bonds with a distance of 1.79 and 1.32 Å (1.89 Å), respectively (Table 4 and Figure 3c). A similar binding mode was shown for the natural product garcinol only recently.[33]

In addition, the chemical structure of the positive control RDS1759 showed a high affinity for the binding site of the HIV-1 RNase H domain (PDB ID: 3K2P), which was confirmed by the average score energy of -8.514 kcal mol^{-1}. RDS1759 formed four hydrogen bonds: two conventional bonds with ARG557(A) and ASP498(A) (distances: 3.09 and 2.36 Å, respectively) and two carbons with ASN474(A) and ASP498(A) (distances: 2.90 and 3.00 Å, respectively). Another π -donor H-bond was established between this compound and ASN474(A) with a distance of 2.78 Å. RDS1759 also formed three metal-acceptor bonds (with Mn^{+2}) with distances of 2.83, 2.03, and 1.91 Å (Table 4 and Figure 3d). Additionally, one electrostatic interaction with ARG557(A) and two hydrophobic interactions with ALA538(A) and ALA445(A) were observed (Table 4 and Figure 3d).

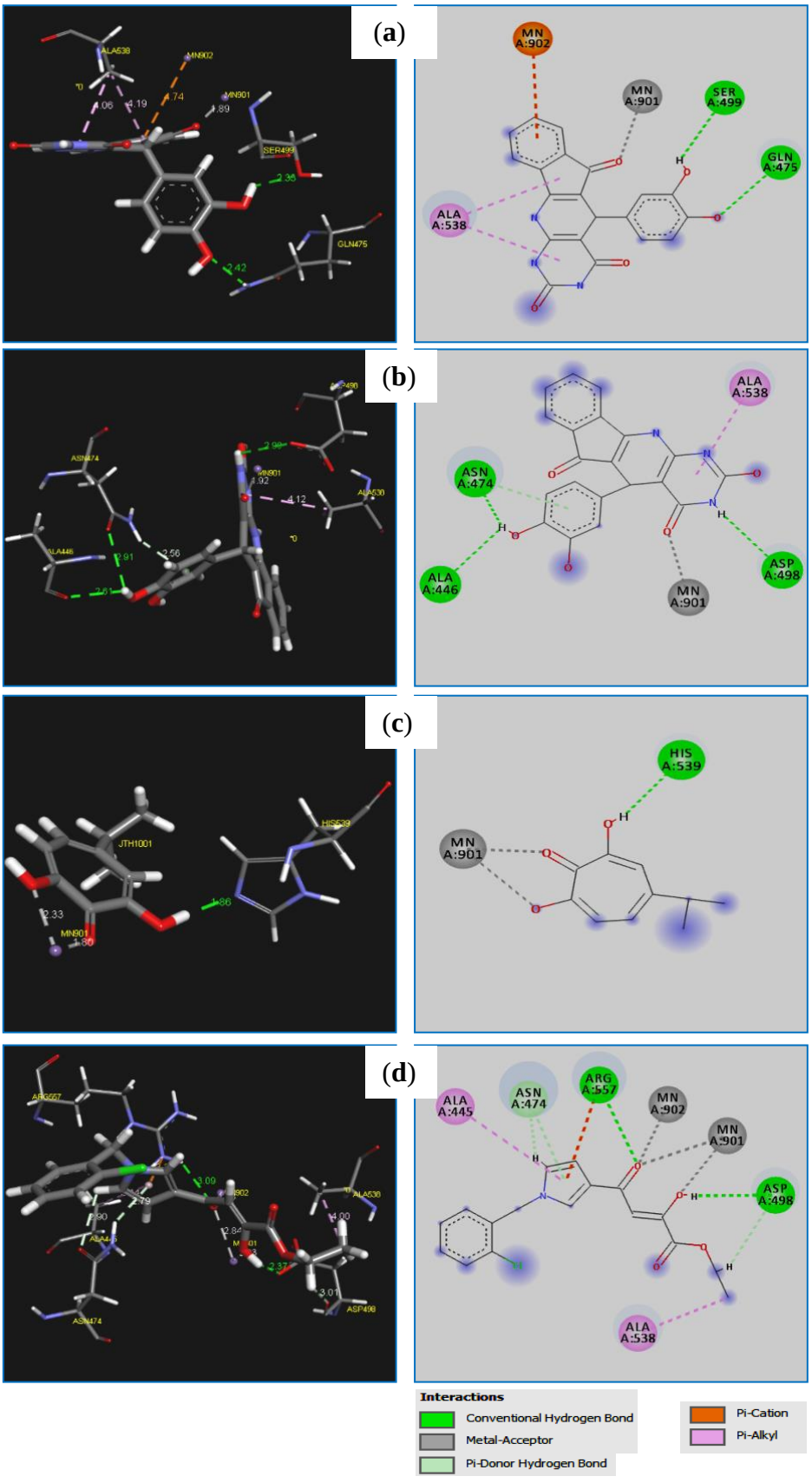

Fig. 3. The 3D and 2D visualization of docked posed structure of the selected ligands with HIV-1 RNase H (PDB: 3K2P); (**a**): **IPU1**, (**b**): **IPU2**, (**c**): β-thujaplicinol, (d): RDS1759.

ADME-T predictions, physicochemical property calculations and drug-likeness evaluation of the **2a**-tautomer **IPU1** were performed using these online servers: SwissADME (http://www.swissadme.ch/) and pkCSM (http://biosig.unimelb.edu.au/pkcsm/prediction). The results are given in Table 5.

Table 5. ADME-T prediction and physicochemical properties of **2a** (**IPU1** tautomer), **2i**, and **2m**.

Entry	TPSA Å²	n-ROTB	MW g/mol	MLog P / WLog P	n-ON acceptors	n-OHNH donors	Rules		
							Lipinski	Veber	Ghose
Rule	**<140**	**<11**	**<500**	**≤5**	**<10**	**<5**	/	/	/
2a	135.28	1	375.33	1.23 / 1.07	5	5	Accepted	Accepted	Accepted
2i	104.05	2	452.26	2.16 / 2.43	**4**	**3**	Accepted	Accepted	Accepted
2m	113.28	3	437.83	1.74 / 2.33	5	3	Accepted	Accepted	Accepted

ADME-T	Absorption		Distribution		Metabolism			Excretion		Toxicity	
	Caco2 (10^{-6} cm/s)	HIA %	CNS (logPS)	BBB (log BB)	CYP1A2 inhibitor	CYP2C19 inhibitor	CYP2D6 substrate	Renal OCT2 substrate	Total Clearance (mL/min/kg)	AMES toxicity	hERG Inhibitor
2a	-0.394	84.5	-2.575	-0.706	YES	YES	NO	NO	0.121	NO	NO
2i	0.999	96.7	-2.231	-0.822	YES	YES	NO	NO	-0.101	YES	NO
2m	0.544	99.1	-2.395	-0.998	YES	YES	NO	NO	0.217	YES	NO

ABS: Absorption**, TPSA:** Topological polar surface area**, n-ROTB:** Number of rotatable bonds**, MW:** Molecular weight**, MLog *P*:** logarithm of partition coefficient of compound between n-octanol and water, **n-ON acceptors:** Number of hydrogen bond acceptors, **n-OHNH donors:** Number of hydrogen bonds donors**.**
Caco-2: Colon adenocarcinoma**, HIA:** Human intestinal absorption**, CNS**: Central nervous system permeability**, BBB:** Blood–brain–barrier permeability**.**
Green = Good**, Red =** Bad**.**

According to the results presented in Table 5, the compounds **2a** (**IPU1** tautomer), **2i** and **2m** show no violations and comply with the Lipinski, Veber and Ghose rules. These compounds also showed a considerable permeability of the cellular plasma membrane and the blood-brain

barrier (BBB). They revealed a very useful parameter for the transport of drug molecules because their TPSA values are lower than 140 $Å^2$.

Based on their high HIA values (> 70%), **2a** (**IPU1**), **2i** and **2m** are expected to be strongly absorbed in the gastrointestinal system to the bloodstream when they are administered orally. The logPS values for **2a** (**IPU1**), **2i** and **2m** are -3< logPS<-2, which means that they can penetrate the CNS. The logBB values are -0.706, -0.822, and -0.998 for **2a** (**IPU1**), **2i** and **2m**, which are > -1, indicating a readily crossing of the blood–brain barrier.

In addition, its high Caco-2 value greater than -5.15 (> -5.15 cm/s) indicates that it has no considerable carcinogenic potential. The **IPU1** tautomer of **2a**, as well as **2i** and **2m**, are negative for AMES and, thus, they are not mutagenic.

2a (**IPU1**), **2i**, and **2m** can be an inhibitor of the CYP1A2 and CYP2C19 isoforms. However, they are not a substrate of CYP2D6. **2a**, **2i** and **2m** are likely not an OCT2 substrate either. Besides, these compounds have low excretion potential with a clearance rate below 5 mL/min/kg. In addition to that, they are no hERG inhibitors (Table 5).

4. Conclusions

Various pyrido- and dihydropyrido[2,3-*d*]pyrimidine derivatives were identified as potent antiparasitic agents in the described activity tests with *T. gondii* and *L. major* parasites. Four compounds (**2m–o**, **3m**) were highly active against *T. gondii* cells at doses of the nanomolar range, albeit without selectivity for these parasites as to test results from non-malignant Vero kidney cells. Hence, structural modifications of pyrido- and dihydropyrido[2,3-*d*]pyrimidines in future works should aim at increased selectivities for *T. gondii* parasites in order to acquire reasonable drug candidates for the treatment of *T. gondii* infections. Alternatively, suitable formulations of these compounds, eventually with parasite-targeting properties, can be rational

strategies in order to reach advanced stages of antiparasitic activity evaluation in living organisms.

Interestingly, certain compounds (**2e**, **2i**, **2m**, **3e**, **3l**) showed distinctly higher activities against *L. major* amastigotes than against promastigotes. This finding is of significance for the potential of this compound class as future antileishmanials. Again, additional optimisation of these compounds appears to be necessary in terms of selectivity for *L. major* amastigotes in order to reduce side-effects.

Catechol **2a**, which displayed only weak antiparasitic activities, showed significant HIV-1 RT-associated RNase H inhibitory activity and docking calculations revealed the relevance of 1,2-dihydroxy-3-nitrophenyl moiety. Thus, the antiviral activity of **2a** is worth further exploration in *ex vivo* and *in vivo* models, with the perspective of its formulation as a cost-effective HIV treatment, in particular, in cases where resistance of RT occurred.

Both tautomers of **2a** dubbed as **IPU1** and **IPU2** can be considered as lead candidates for the inhibition of the HIV-1 RNase H domain. They established several interactions with active site residues of the HIV1 RNase H domain as to docking calculations. Thus, results obtained from molecular docking supported the potential of **2a**, especially in its **IPU1** tautomer form, as a promising new HIV-1 RNase H inhibitor. ADME-T prediction and physicochemical properties were calculated to verify the pharmacodynamics and pharmacokinetics, and the results proved that **2a**, **2i**, and **2m** comply with the Lipinski, Veber and Ghose rules.

Declaration of Competing Interest

The authors declare that they have no known competing financial interests or personal relationships that could have appeared to influence the work reported in this paper.

Data availability

Data will be made available on request.

Abbreviations

ADME-T	Absorption, distribution, metabolism, excretion - toxicity
AmB	Amphotericin B
ATO	Atovaquone
BBB	Blood brain barrier
CL	Cutaneous leishmaniasis
CNS	Central nervous system
CYP	Cytochrome P
FBS	Fetal bovine serum
hERG	Human ether-à-go-go-related gene
HIA	Human intestinal absorption
HIV	Human immunodeficiency virus
MCL	Mucocutaneous leishmaniasis
MW	Molecular weight
NTD	Neglected tropical disease
OCT2	Organic cation transporter 2
PDB	Protein data bank
ROTB	Rotable bonds
RT	Reverse transcriptase
RPMI	Roswell Park Memorial Institute
SI	Selectivity index

TPSA	Topological polar surface area
VL	Visceral leishmaniasis

Acknowledgements

A. C. and E. T. were supported by Regione Autonoma della Sardegna (RAS) (LR 07/2017, annualità 2017) grant no. RASSR17032.

Appendix A. Supplementary data

Supplementary data to this article can be found online at https://doi.org/0000.

References

1. Baker RE, Mahmud AS, Miller IF, Rajeev M, Rasamainarivo F, Rice BL, Takahashi S, Tatem AJ, Wagner CE, Wang L-F, Wesolowski A, Metcalf CJE. Infectious disease in an era of global change. *Nat Rev Microbiol.* 2022;20:193–205.
2. Mitra AK, Mawson AR. Neglected tropical diseases: epidemiology ad global burden. *Trop Med Infect Dis.* 2017;2:36.
3. Kampf G, Brüggemann Y, Kaba HEJ, Steinmann J, Pfaender S, Scheithauer S, Steinmann E. Potential sources, modes of transmission and effectiveness of prevention measures against SARS-CoV-2. *J Hospit Infect.* 2020;106:678–697.
4. http://www.who.int/mediacentre/factsheets/fs375/en/; Accessed November 12, 2020.
5. van Bocxlaer K, Caridha D, Black C, Vesely B, Leed S, Sciotti RJ, Wijnant G-J, Yardley V, Braillard S, Mowbray CE, Ioset J-R, Croft SL. Novel benzoxaborole, nitroimidazole and aminopyrazoles with activity against experimental cutaneous leishmaniasis. *IJP: Drugs Drug Resist.* 2019;11:129–138.

6. Bennis I, Belaid L, de Brouwere V, Filali H, Sahibi H, Boelart M. ´´The mosquitoes that destroy your face´´: social impact of cutaneous leishmaniasis in south-eastern Morocco, a quality study. *PLoS One.* 2017;12:e0189906.
7. Kassi M, Afghan A, Rehman R, Kasi PM. Marring leishmaniasis: the stigmatization and the impact of cutaneous leishmaniasis in Pakistan and Afghanistan. *PLoS Negl Trop Dis.* 2008;2:e259.
8. Al Nasr I, Ahmed F, Pullishery F, El-Ashram S, Ramaiah VV. Toxoplasmosis and anti-*Toxoplasma* effects of medicinal plant extracts – a mini-review. *Asian Pac J Trop Med.* 2016;9:730–734.
9. Cohen J. Combo of two HIV vaccines fails its big tests. *Science.* 2020;367:611–612.
10. Henderson LJ, Reoma LB, Kovacs JA, Nath A. Advances toward curing HIV-1 infection in tissue reservoirs. *J Virol.* 2018;94:1–21.
11. Menéndez-Arias L. Molecular basis of human immunodeficiency virus type 1 drug resistance: overview and recent developments. *Antivir Res.* 2013;98:93–120.
12. Stella-Ascariz N, Arribas JR, Paredes R, Li JZ. The role of HIV-1 drug-resistant minority variants in treatment failure. *J Infect Dis.* 2017;216:S847–S850.
13. Gupta RK, Gregson J, Parkin N, Haile-Selassie H, Tanuri A, Andrade Forero L, Kaleebu P, Watera C, Aghokeng A, Mutenda N, Dzangare J, Hone S, Hang ZZ, Garcia J, Garcia Z, Marchorro P, Beteta E, Giron A, Hamers R, Inzaule S, Frenkel LM, Chung MH, de Oliveira T, Pillay D, Naidoo K, Kharsany A, Kugathasan R, Cutino T, Hunt G, Rios SA, Doherty M, Jordan MR, Bertagnolio S. HIV-1 drug resistance before initiation or re-initiation of first-line antiretroviral therapy in low-income and middle-income countries: a systematic review and meta-regression analysis. *Lancet Infect Dis.* 2017;18:346–355.

14. Alvar J, Aparicio P, Aseffa A, Den Boer M, Canavate C, Dedet J-P, Gradoni L, Ter Horst R, López-Vélez R, Moreno J. The relationship between leishmaniasis and AIDS: the second 10 years. *Clin Microbiol Rev.* 2008;21:334–359.
15. Singh KP, Crane M, Audsley J, Avihingsanon A, Sasadeusz J, Lewin SR. HIV-hepatitis B virus coinfection: epidemiology, pathogenesis, and treatment. *AIDS*. 2017;31:2035–*2052.
16. Le Grice SF. Human immunodeficiency virus reverse transcriptase: 25 years of research, drug discovery, and promise. *J Biol Chem.* 2012;287:40850–40857.
17. Nowotny M, Yang W. Stepwise analyses of metal ions in RNase H catalysis from substrate destabilization to product release. *EMBO J.* 2006;25:1924–1933.
18. Rosta E, Yang W, Hummer G. Calcium inhibition of ribonuclease H1 two-metal ion catalysis. *J Am Chem Soc.* 2014;136:3137–3144.
19. Tramontano E, Corona A, Menéndez-Arias L. Ribonuclease H, an unexploited target for antiviral intervention against HIV and hepatitis B virus. *Antiviral Res.* 2019;171:104613.
20. Esposito F, Sanna C, Del Vecchio C, Cannas V, Venditti A, Corona A, Bianco A, Serrilli AM, Guarcini L, Parolin C, Ballero M, Tramontano E. *Hypericum hircinum* L. components as new single-molecule inhibitors of both HIV-1 reverse transcriptase-associated DNA polymerase and ribonuclease H activities. *Pathog Dis.* 2013;68:116–124.
21. Xu L, Grandi N, Del Vecchio C, Mandas D, Corona A, Piano D, Esposito F, Parolin C, Tramontano E. From the traditional Chinese medicine plant *Schisandra chinensis* new scaffolds effective on HIV-1 reverse transcriptase resistant to non-nucleoside inhibitors. *J Microbiol.* 2015;53:288–293.
22. Sanna C, Scognamiglio M, Fiorentino A, Corona A, Graziani V, Caredda A, Cortis P, Montisci M, Ceresola ER, Canducci F, Poli F, Tramontano E, Esposito F. Prenylated

phloroglucinols from *Hypericum scruglii*, an endemic species of Sardinia (Italy), as new dual HIV-1 inhibitors effective on HIV-1 replication. *PLoS ONE.* 2018;13:e0195168.

23. Schneider A, Corona A, Spöring I, Jordan M, Buchholz B, Maccioni E, di Santo R, Bodem J, Tramontano E, Wöhrl BM. Biochemical characterization of a multi-drug resistant HIV-1 subtype AG reverse transcriptase: antagonism of AZT discrimination and excision pathways and sensitivity to RNase H inhibitors. *Nucleic Acids Res.* 2016;44:2310–2322.
24. Corona A, Ballana E, Distinto S, Rogolino D, Del Vecchio C, Carcelli M, Badia R, Riveira-Munoz E, Esposito F, Parolin C, Esté JA, Grandi N, Tramontano E. Targeting HIV-1 RNase H: N'-(2-hydroxy-benzylidene)-3,4,5-trihydroxybenzoylhydrazone as selective inhibitor active against NNRTIs-resistant variants. *Viruses.* 2020;12:729.
25. Botta L, Cesarini S, Zippilli C, Bizzarri BM, Fanelli A, Saladino R. Multicomponent reactions in the synthesis of antiviral compounds. *Curr Med Chem.* 2022;29:2013–2050.
26. Evdokimov NM, Van Slambrouck S, Heffeter P, Tu L, Le Calvé B, Lamoral-Theys D, Hooten CJ, Uglinskii PY, Rogelj S, Kiss R, Steelant WFA, Berger W, Yang JJ, Bologa CG, Kornienko A, Magedov IV. Structural simplification of bioactive natural products with multicomponent synthesis. 3. Fused uracil-containing heterocycles as novel topoisomerase-targeting agents. *J Med Chem.* 2011;54:2012–2021.
27. Marat X, Muller B, Thomas-Collignon A, Bernard D. Active compounds for combating greasy skin. *Eur Pat.* 2016;EP 2 858 623 B1.
28. Jelali H, Al Nasr I, Koko W, Khan T, Deniau E, Sauthier M, Hamdi N. Synthesis, characterization and in vitro bioactivity studies of isoindolin-1-3-phosphonate compounds. *J Heterocycl Chem.* 2021;doi: 10.1002/jhet.4396.
29. Osorio E, Arango G, Jiménez N, Alzate F, Ruiz G, Gutiérrez D, Robledo S. Antiprotozoal and cytotoxic activities in vitro of Colombian Annonaceae. *J Ethnopharmacol.* 2007;111:630–635.

30. Al Nasr I, Hanachi R, Said R, Rahali S, Tangour B, Abdelwahab SI, Farasani A, Taha MME, Bidwai A, Koko WS, Khan TA, Schobert R, Biersack B. p-Trifluoromethyl- and p-pentafluorothio-substituted curcuminoids of the 2,6-di[(E)-benzylidene)]cycloalkanone type: syntheses and activities against *Leishmania major* and *Toxoplasma gondii* parasites. *Bioorg Chem.* 2021;114:105099.
31. Koko WS, Mesaik MA, Yousaf S, Galal M, Choudhary MI. In vitro immunomodulating properties of selected Sudanese medicinal plants. *J Ethnopharmacol.* 2008;118:26–34.
32. Corona A, Schneider A, Schweimer K, Rösch P, Wöhrl BM, Tramontano E. Inhibition of foamy virus reverse transcriptase by human immunodeficiency virus type I RNase H inhibitors. *Antimicrob Agents Chemother.* 2014;58:4086–4093.
33. Corona A, Seibt S, Schaller D, Schobert R, Volkamer A, Biersack B, Tramontano E. Garcinol from *Garcinia indica* inhibits HIV-1 reverse transcriptase-associated ribonuclease H. *Arch Pharm.* 2021;354:e2100123.
34. Frisch MJ, Trucks GW, Schlegel HB, Scuseria GE, Robb MA, Cheeseman JR, Scalmani G, Barone V, Petersson GA, Nakatsuji H, Li X, Caricato M, Marenich AV, Bloino J, Janesko BG, Gomperts R, Mennucci B, Hratchian HP, Ortiz JV, Izmaylov AF, Sonnenberg JL, Williams-Young D, Ding F, Lipparini F, Egidi F, Goings J, Peng B, Petrone A, Henderson T, Ranasinghe D, Zakrzewski VG, Gao J, Rega N, Zheng G, Liang W, Hada M, Ehara M, Toyota K, Fukuda R, Hasegawa J, Ishida M, Nakajima T, Honda Y, Kitao O, Nakai H, Vreven T, Throssell K, Montgomery Jr. JA, Peralta JE, Ogliaro F, Bearpark MJ, Heyd JJ, Brothers EN, Kudin KN, Staroverov VN, Keith TA, Kobayashi R, Normand J, Raghavachari K, Rendell AP, Burant JC, Iyengar SS, Tomasi J, Cossi M, Millam JM, Klene M, Adamo C, Cammi R, Ochterski JW, Martin RL, Morokuma K, Farkas O, Foresman JB, Fox DJ. Gaussian 16, Revision B.01, Gaussian Inc. Wallingford CT, 2016.

35. Lee C, Yang W, Parr RG. Development of the Colle-Salvetti correlation-energy formula into a functional of the electron density. *Phys Rev B.* 1988;37:785–789.

36. Grimme S, Antony J, Ehrlich S, Krieg H. A consistent and accurate ab initio parametrization of density functional dispersion correction (DFT-D) for the 94 elements H-Pu. *J Chem Phys.* 2010;132:154104.

37. Krishnan R, Binkley JS, Seeger R, Pople JA. Self-consistent molecular orbital methods. XX. A basis set for correlated wave functions. *J Chem Phys.* 1980;72:650–654.

38. Barone V, Cossi M. Quantum calculation of molecular energies and energy gradients in solution by a conductor solvent model. *J Phys Chem A.* 1998;102:1995–2001.

39. Othmani H, Said RB, Terzi N, Jaidane N-E, Morgren MMA, Elmarghany A, Hochlaf M. Structural, energetic and spectroscopic characterisation of 5-fluorouracil anticarcinogenic drug isomers, tautomers and ions. *Mol Phys.* 2019:117;1589–1603.

40. Said RB, Kolle JM, Essalah K, Tangour B, Sayari A. A unified approach to CO_2–amine reaction mechanisms. *ACS Omega.* 2020;5:26125–26133.

41. Molecular operating environment (MOE), 2013.08. Chemical Computing Group Inc., Montreal, 2016.

42. Daoud I, Melkemi N, Salah T, Ghalem S. Combined QSAR, molecular docking and molecular dynamics study on new acetylcholinesterase and butyrylcholinesterase inhibitors. *Comput Biol Chem.* 2018;74:304–326.

43. Chenafa H, Mesli F, Daoud I, Achiri R, Ghalem S, Neghra A. In silico design of enzyme α-amylase and α-glucosidase inhibitors using molecular docking, molecular dynamic, conceptual DFT investigation and pharmacophore modelling. *J Biomol Struct Dyn.* 2021;40:6308–6329.

44. Himmel DM, Maegley KA, Pauly TA, Bauman JD, Das K, Dharia C, Clark Jr. AD, Ryan K, Hickey MJ, Love RA, Hughes SH, Bergqvist S, Arnold E. Structure of HIV-1

reverse transcriptase with the inhibitor β-thujaplicinol bound at the RNase H active site. *Structure*. 2009;17:1625–1635.

45. Hevener KE, Zhao W, Ball DM, Babaoglu K, Qi J, White SW, Lee RE. Validation of molecular docking programs for virtual screening against dihydropteroate synthase. *J Chem Inf Model.* 2009;49:444–460.
46. Daina A, Michielin O, Zoete V. SwissADME: a free web tool to evaluate pharmacokinetics, drug-likeness and medicinal chemistry friendliness of small molecules. *Sci Rep.* 2017;7:42717.
47. Daina A, Zoete V. A boiled-egg to predict gastrointestinal absorption and brain penetration of small molecules. *ChemMedChem*. 2016;11:1117–1121.
48. Pires DE, Blundell TL, Ascher DB. pkCSM: predicting small-molecule pharmacokinetic and toxicity properties using graph-based signatures. *J Med Chem.* 2015;58:4066–4072.
49. McLoughlin EC, O'Boyle NM. Colchicine-binding site inhibitors from chemistry to clinic: a review. *Pharmaceuticals*. 2020;13:8.
50. Vermeersch M, da Luz RI, Toté K, Timmermans J-P, Cos P, Maes L. In vitro susceptibilities of *Leishmania donovani* promastigote and amastigote stages to antileishmanial reference drugs: practical relevance of stage-specific differences. *Antimicrob Agents Chemother*. 2009;53:3855–3859.
51. Kirby KA, Myshakina NA, Christen MT, Chen Y-L, Schmidt HA, Huber AD, Xi Z, Kim S, Rao RK, Kramer ST, Yang Q, Singh K, Parniak MA, Wang Z, Ishima R, Sarafianos SG. A 2-hydroxyisoquinoline-1,3-dione active-site RNase H inhibitor binds in multiple modes to HIV-1 reverse transcriptase. *Antimicrob Agents Chemother*. 2017;61:e01351–17.

52. Imberty A, Hardman KD, Carver JP, Pérez S. Molecular modelling of protein-carbohydrate interactions. Docking of monosaccharides in the binding site of concanavalin A. *Glycobiology*. 1991;1:631–642.
53. Jeffrey GA. *An introduction to hydrogen bonding*. Vol. 12. New York, NY: Oxford University Press; 1997.
54. Zhang B, D'Erasmo MP, Murelli RP, Gallichio E. Free energy-based virtual screening and optimization of RNase H inhibitors of HIV-1 reverse transcriptase. *ACS Omega*. 2016:1:435–447.

Highlights

- 1*H*-Indeno[2',1':5,6]dihydropyrido[2,3-*d*]pyrimidine and 1*H*-indeno[2',1':5,6]pyrido[2,3-*d*]pyrimidine derivatives were prepared.
- High activity against *Toxoplasma gondii* parasites and *Leishmania major* amastigotes was observed.
- A catechol derivative inhibits HIV-1 RT-associated RNase H.
- Docking and ADME-T calculations confirmed drug-like properties of active compounds.

Graphical Abstract

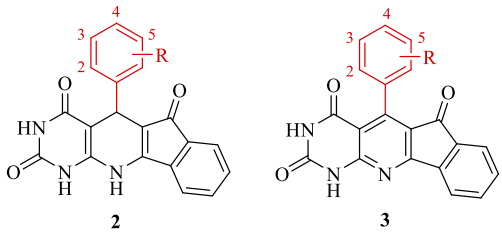

- *Simple preparation*
- *Active against T. gondii and L. major*
- *Inhibition of HIV-1 RT-associated RNase H*